

CDM mechanisms-based modelling of tertiary creep: ability to predict the life of engineering components

D. R. HAYHURST

*The University of Manchester,
School of Mechanical, Aerospace and Civil Engineering,
Manchester, U.K.*

THE PAPER demonstrates how computational CDM can be used to predict the behaviour of structural components, ranging from modest stress concentrators to the growth of cracks by creep. Size effects in CDM analysis are addressed, and it is shown how a non-local CDM approach can be used to predict the observed crack tip behaviour. The proviso being that the length scales, associated with the damage fields and gradients, be modelled to comply with continuum theory. It is shown how damage state variable theories may be used to provide traceability from the physics of micro-mechanisms to the macro-material behaviour described by constitutive equations. The paper presents a detailed analysis of creep rupture in ferritic steel weldments, and shows how multi-axial stress rupture criteria, weldment phase dimensions, and constitutive equations for each material phase of the weld, can be used in Finite Element CDM analyses to predict the results of experiments carried out on butt-welded pipes and cross-welded tension testpieces. Original results are presented which show how the above CDM techniques have been used to perform a three-dimensional CDM high-temperature creep rupture analysis of a welded cylinder-cylinder pressure vessel intersection; and, to predict damage initiation and crack growth. The paper also demonstrates how CDM conservatively predicts the vessel lifetime; and, how the experimentally observed weld failure mechanism is well predicted.

Notations

ε_{ij}	creep strain tensor,
σ_{ij}	stress tensor,
ω_i	i -th damage variable,
ω_n	n -th damage variable,
s_{ij}	deviatoric stress tensor,
δ_{ij}	Kronecker Delta,
σ_e	effective stress $\left(= (3s_{ij}s_{ij}/2)^{1/2} \right)$,
ε_e	effective strain $\left(= (2\varepsilon_{ij}\varepsilon_{ij}/3)^{1/2} \right)$,
σ_1	maximum principal tension stress,
σ_o	normalizing stress,
$\Delta(\sigma_{ij})$	damage rate stress function,
J_1	first stress invariant $(= \sigma_{ii})$,

- H primary creep state variable,
 Φ particle coarsening damage variable,
 ω creep constrained cavity growth damage variable,
 α, ν multi-axial stress rupture parameters,
 T temperature $^{\circ}\text{K}$.

Functions

- N Heaviside unit function,
 f strain rate functional,
 g_i i -th damage rate functional.

Normalisation

- Σ_{ij} normalized stress tensor ($= (\sigma_{ij}/\sigma_o)$),
 Σ_1 normalized maximum principal stress ($= (\sigma_1/\sigma_o)$),
 Σ_e normalized effective stress ($= (\sigma_e/\sigma_o)$).

Material Constants

- K strain rate constant,
 n strain rate stress exponent,
 m time exponent,
 M damage rate constant,
 χ damage rate stress exponent,
 ϕ damage function exponent,
 A strain rate constant,
 B sinh function stress dependence,
 C damage rate constant,
 h primary creep constant,
 H^* saturation value of primary creep variable,
 K_c particle coarsening variable,
 a, b constants in multi-axial stress rupture parameter equation.

Geometry

- κ crack depth,
 β half specimen width,
 \hat{A} area of cell or finite element
 θ angular location of branch diametral plane, relative to crotch section
 $\theta = 0^{\circ}$ (flank section $\theta = 90^{\circ}$),
 R/t_p ratio of mean radius to main pipe thickness,
 r/t_b ratio of mean radius to branch thickness.

Weld Zone Notation

- CG-HAZ coarse grained bainite region,
 R-HAZ refined/fine grained bainite,
 Type IV intercritical, original and refined equi-axed, ferrite/bainite of differing proportions.

Superscripts

- \cdot time rate of change.

Subscripts

- ij indices of stress and strain tensor,
- l maximum principal tension stress,
- e effective stress and strain,
- cell relates to damage cell,
- el relates to finite element,
- * primary creep saturation value,
- r rupture or failure value.

1. Introduction

High-temperature design in the creep range of metallic components is largely carried out using design by code methods, e.g. BS 806, 1113, 5500 [1, 2, 3], ASME CODE CASE N47-29 [4] or by design assessment routes, e.g. R5 [5]. However, flexibility is provided within the codes for the designer to use design by analytic methods. The latter are essential in situations where the designer operates on or beyond the boundaries of applicability. It is in these cases where new and more accurate methods of analysis have appeal.

The theme of this paper is the use of computational Continuum Damage Mechanics (CDM) with the finite element method to predict a broad range of structural and component behaviours from simple uni-axial creep data; and, to demonstrate that the approach is capable of predicting creep crack growth rates in complex structures. Shown schematically in Fig. 1 is a range of structures of increasing complexity, starting on the left-hand side with a uniformly stressed bar, to a plane stress plate containing a hole, to a Bridgman notched bar with its throat area subjected to complex tri-axial stresses, to a plane strain double-

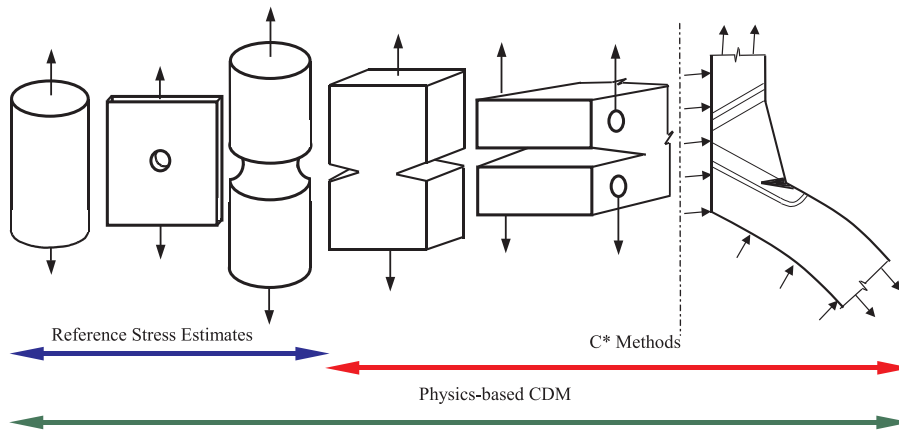


FIG. 1. Schematic representation of the range of increasingly complex structures which have been analysed using CDM and C* techniques.

edged notched tension bar, to a Compact Tension Specimen, CTS, and finally on the right, to an axi-symmetrically welded sphere-cylinder intersection subjected to internal pressure. It will be shown how the reference stress techniques can be used to predict lifetimes and deformation behaviour within a CDM framework, and extended to determine creep crack growth in the three remaining structures on the right-hand side of the figure. The prediction of the behaviour of the latter has been traditionally regarded as being achievable only by using the nonlinear fracture mechanics parameter C^* [6, 7]. The requirement for the use of computational CDM in creep crack growth analyses is that length scales associated with damage fields and gradients should be modelled to comply with continuum theory. The CDM approach has the advantage of providing traceability from the constitutive equations used, through the physics of the deformation, damage and fracture processes involved, to the fundamental microstructural behaviour.

The paper commences with an outline of CDM. This is followed by an overview of the generic approach to design provided by computational CDM using the finite element technique. The paper then considers the prediction of creep crack growth using CDM, and a treatment of size effects in creep crack growth; it is shown how the arrangement and size of the finite elements have to be correctly modelled to capture length scales and gradients associated with damage. The paper then addresses the application of CDM computational techniques to the prediction of creep failure in ferritic steel welds in butt-welded pipes, uniaxially loaded cross-welded testpieces; and finally, new results are presented which demonstrate the power of CDM to predict experimentally observed damage, failure patterns, and lifetimes in a welded branched cylinder-cylinder pressure vessel intersection.

2. What is CDM?

HAYHURST [8] has shown that macrocracks form in creep rupture from relatively uniform fields of grain boundary microcracks. What is evident is that a single crack does not predominate and propagate across the section. HAYHURST [9] has shown from this and other studies, that provided the stress field is homogeneous, then a field of damage nucleates and grows in a uniform way over the same region. The strain rate behaviour and the damage evolution rate behaviour may be described by the following equations:

$$\begin{aligned}
 \dot{\epsilon}_{ij} &= f(\sigma_{ij}, \omega_1, \omega_2, \dots, \omega_n, T), \\
 \dot{\omega}_1 &= g_1(\sigma_{ij}, \omega_1, \omega_2, \dots, \omega_n, T), \\
 \dot{\omega}_2 &= g_2(\sigma_{ij}, \omega_1, \omega_2, \dots, \omega_n, T),
 \end{aligned}
 \tag{2.1}$$

$$(2.1) \quad \begin{array}{c} \vdots \\ \vdots \\ \vdots \end{array}$$

[cont.]

$$\dot{\omega}_n = g_n(\sigma_{ij}, \omega_1, \omega_2, \dots, \omega_n, T),$$

where $\dot{\omega}_1, \dot{\omega}_2, \dots, \dot{\omega}_n$ are rates of change of the damage state variables and T is the temperature in °K. The damage state variables could include the following: cavity nucleation and growth; ductile void growth; multiplication of dislocation substructures; and precipitate coarsening [10–12]. A number of papers [13–17] have reported contributions to the establishment of Computational Continuum Damage Mechanics as a route to high-temperature design analysis

3. CDM: Predictive capability

3.1. Stress redistribution due to CDM

Shown in Fig. 2 is a mid-thickness micrograph of part of a quarter section of a copper tension panel tested at 523°K immediately prior to failure. The plate contained a central circular hole, part of which is shown in the bottom right-hand corner of the figure. The left-hand boundary of the figure is of a region close to the edge of the plate. The top boundary of the figure is subjected to a remote steady uniform tension. It is evident from Fig. 2 that widespread continuum damage has taken place; and, the CDM calculations reported by HAYHURST *et al.* [14] show that damage formation is accompanied by considerable stress redistribution which, shortly after load up, produces an almost uniform stress across the minimum load bearing section of the plate. This leads to the result that the lifetime of the plate may be computed using the net section stress and uni-axial creep rupture data. The average experimental lifetimes are greater than the computed

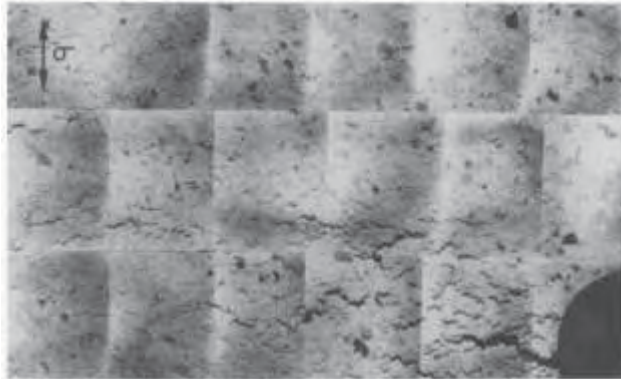


FIG. 2. Micrograph of a section of a part of quarter-section of a copper tension panel, tested at 523°K, containing a central circular hole. The test was stopped just before failure.

lifetimes by amounts equivalent to 3% and 7% on stress for the aluminium alloy and copper plates respectively. This result clearly shows the highly beneficial effects of stress redistribution, a similar plate was tested [18] in which the hole was replaced by a narrow slit of the same characteristic dimension. Again it was shown that stress redistribution rapidly nullified the initial high stress and strain gradients at the tip of the slit, and that the lifetime of the plate could again be predicted using the netsection stress and uni-axial creep rupture data. The average experimental lifetimes are less than the computed lifetimes by amounts equivalent to 1% and 2% on stress respectively for the aluminium and copper plates containing slits. This result holds provided that the material behaves so that a major part of the strain is accumulated during tertiary creep [19].

3.2. Multi-axial stress rupture criteria

The creep rate Eq. (2.1) is given by:

$$(3.1) \quad \dot{\epsilon}_{ij} = 3K\sigma_e^{n-1}s_{ij}t^m/2(1-\omega)^n,$$

where $s_{ij} = \sigma_{ij} - \delta_{ij}\sigma_{kk}/3$, and K , m and n are material constants. A single damage rate Eq. (2.1) is given by:

$$(3.2) \quad \dot{\omega} = M\Delta^x(\sigma_{ij})t^m/(1+\phi)(1-\omega)^\phi,$$

where $\Delta(\sigma_{ij})$ is the stress function $\{\alpha\sigma_1 + (1-\alpha)\sigma_e\}$, α , ϕ and M are material constants. Equation (3.2), due to SDOBYREV [20], can be normalised with respect to the uni-axial stress σ_o to yield normalised stresses $\Sigma_{ij} = \sigma_{ij}/\sigma_o$, $\omega = 0$ at $t = 0$, and $\omega = 1$ at failure to give:

$$(3.3) \quad \Delta(\Sigma_{ij}) = 1 = \{\alpha\Sigma_1 + (1-\alpha)\Sigma_e\},$$

which defines the isochronous rupture surface in normalised stress space in terms of the parameter α [8].

In this section two materials will be discussed having different multi-axial stress rupture criteria. They are copper, for which $\alpha = 0.83$ [16] which is approximately described by a maximum principal tension stress rupture criteria; and, an aluminium alloy for which $\alpha = 0$, which is described by an effective stress rupture criterion [8]. Both will be considered in this section when tested in an axi-symmetrically notched tension bar. The latter have been established as a practical laboratory technique for subjecting materials to high values of the first stress invariant $J_1 (= \sigma_{ii})$ and to low values of the effective stress σ_e .

A micrograph of a diametrical plane taken from a copper circular notched bar tested at 523 °K until just before failure is shown in Fig. 3. The figure shows a uniform state of damage which is synonymous with a relatively uniform state

of stress and strain in the centre of the notch throat. This observation provides the justification for the use of the BRIDGMAN testpiece [21] as a means of subjecting a relatively large volume of material to a relatively uniform state of complex stress.

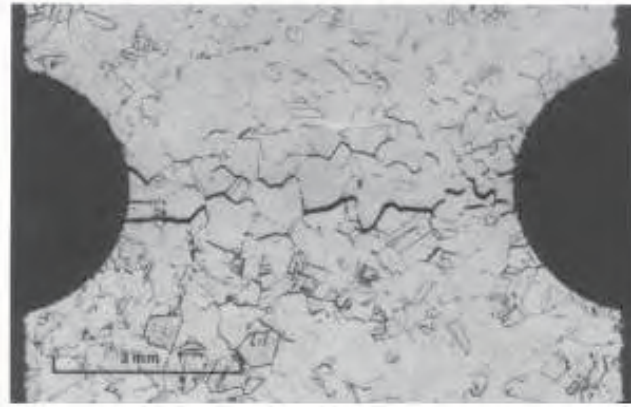


FIG. 3. Micrograph of a diametral plane taken from an axi-symmetrically notched copper specimen tested at 523°K almost to failure under tension.

Copper and aluminium notched bars when creep tested in this way show slight notch weakening and notch strengthening respectively. That is, for notch strengthening the specimen has a rupture lifetime in excess of the lifetime of a plain bar tested at the net section stress. Copper shows typically 2% notch weakening and the aluminium alloy shows approximately 28% notch strengthening. As shown by HAYHURST *et al.* [16], CDM is capable of predicting these results using Eqs. (3.1) and (3.2). The success of the approach is entirely dependent upon a knowledge of accurate values of the multi-axial stress rupture criterion α for both materials.

In design terms this is an important result, since in components which involve changes in section, and root radii, complex stress states are always generated. For these situations design calculation methods often assume that the rupture criterion is effective stress-controlled ($\alpha = 0$) when in fact, many practical materials have α values approaching unity.

HAYHURST *et al.* [16] have shown that when the circular notched bar geometry is replaced by the British Standard V-notch geometry then damage accumulation behaviour becomes highly localised to the notch root. It is then more akin to damage evolution behaviour observed in creep crack growth. Despite this, CDM was shown [16] to be capable of predicting this localised behaviour and creep rupture lifetimes. This result gave the hint that CDM should be capable of predicting creep crack growth and led to a study of the behaviour of plane strain

double-edged notched tension specimens [22], the results of which are outlined in the next section.

3.3. Prediction of creep crack growth using CDM

A double-edged cracked tension specimen was used to test creep rupture behaviour both in copper and in an aluminium alloy. The CDM prediction showed two dramatically different predictions. The copper testpiece showed a widespread redistribution of stress due to damage growth as shown in Fig. 4(a), the result being that the singularities in stress and strain at the crack tip were rapidly relaxed, and behaviour was quickly established close to that of net section stress control. Specimen lifetimes were very accurately predicted. In the case of the aluminium alloy testpiece the predicted behaviour closely agreed with that observed,

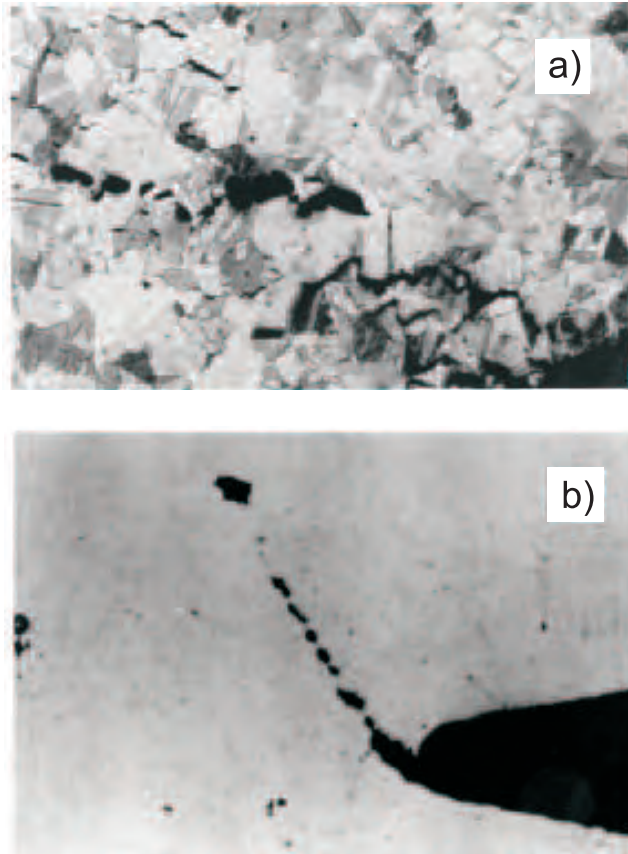


FIG. 4. Mid-thickness micrographs of plane strain double-edge cracked tension specimens just before failure, (a) copper testpiece tested at 523°K and, (b) aluminium alloy testpiece tested at 483°K.

which showed highly localised damage which had grown on a plane inclined at 67° to the notch plane as shown in Fig. 4(b). Close metallographic examination revealed cavity damage growth on grain boundary facets which had linked by a shear instability mechanism on the 67° plane. For the aluminium alloy, which obeyed a maximum effective stress rupture criterion, $\alpha = 0$, this mechanism was clearly stronger than that operating on the plane of the original crack. Damage growth along the 67° plane took place at a decreasing rate until net section behaviour finally took over.

Both of these studies, together with others on stainless steel double-edged cracked specimens, and on compact tension specimens [23], unambiguously demonstrated that CDM computations using the finite element solver DAMAGE XX [14, 16, 22] are capable of predicting creep crack growth from uni-axial creep data and a knowledge of the multi-axial stress rupture criterion of the material. For internally and externally cracked aluminium alloy and copper specimens, the predicted and experimental lifetimes agreed to within an amount equivalent to 1% on stress.

4. Testpiece size effects

The effects of testpiece size have been demonstrated [24] using tests on copper double-edged cracked tension specimens done at 523°K . Large and small, but geometrically similar testpieces were tested with a ratio $\kappa/\beta = 0.667$, where κ is the crack depth and β is the specimen half width. For the large testpiece $\kappa = 12.7$ mm, and the small testpiece is half scale. The nominal, notch throat, stress was 40 MPa. The lifetimes for the geometrically similar testpieces are given in Table 1. The small testpiece have a lifetime 500 h longer than the larger one. Conventional CDM analysis techniques are not able to predict the difference in lifetimes; a single value of 1600 h being predicted.

Table 1. Comparison of predicted and experimental lifetimes for large and small copper double-edged notched tension specimens at 523°K .

Testpiece	Experiment	Predicted
Large	1300 h	1390 h
Small	1800 h	1850 h

HALL and HAYHURST [24] showed how a length scale can be introduced into the CDM calculation. Shown in Fig. 5 is the introduction of a square cell mesh whose corner is located near the notch tip. The cell size is the same, i.e. 0.9 mm for both testpieces. The cell size has been determined from the “rule of thumb” that repeatable continuum uni-axial rupture properties independent of size can be measured in testpieces that have 6–7 grains across a testpiece bar diameter.

The cell damage rate in the CDM analysis has been computed using:

$$(4.1) \quad \dot{\omega}_{\text{cell}} = \frac{1}{\widehat{A}_{\text{cell}}} \int_{\widehat{A}_{\text{cell}}} \dot{\omega}_{\text{el}} d\widehat{A}_{\text{el}},$$

$$\widehat{A}_{\text{cell}} = \int_{\widehat{A}_{\text{cell}}} d\widehat{A}_{\text{el}},$$

and for finite elements which fall on the cell boundaries the contribution within the cell is given by:

$$(4.2) \quad \dot{\omega}_{\text{el}} = \frac{1}{\widehat{A}_{\text{el}}} \int_{\widehat{A}_{\text{el}}} \dot{\omega}_{\text{cell}} d\widehat{A}_{\text{cell}}.$$

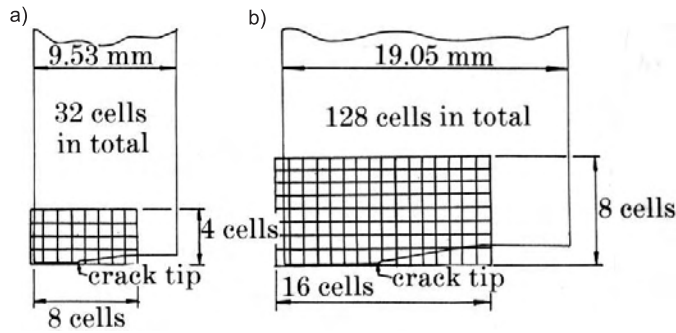


FIG. 5. Cell meshes used to overlay the finite element meshes representing a) small, b) large externally cracked testpieces. Square cell side dimension is 0.9 mm.

In this way each cell has a single value of damage rate and damage. However, at the element level, damage rates are different due to the stress and strain gradients associated with the crack tip.

Figures 6a and 6b show damage fields for the small testpiece at life fractions of 0.530 and 0.822 respectively. Figure 6c shows the predicted damage field at failure for the small testpiece; and, Fig. 6d the corresponding mid-thickness micrograph. Close agreement may be observed between predictions and experiment. Figure 6e shows the predicted damage fields at failure for the large testpiece; and Fig. 6f shows the corresponding mid-thickness micrograph at failure; close agreement has been achieved. Comparison of Figs. 6c and 6d with Figs. 6e and 6f show that the latter, for the larger specimen, has damage fields which are more closely confined to the minimum section.

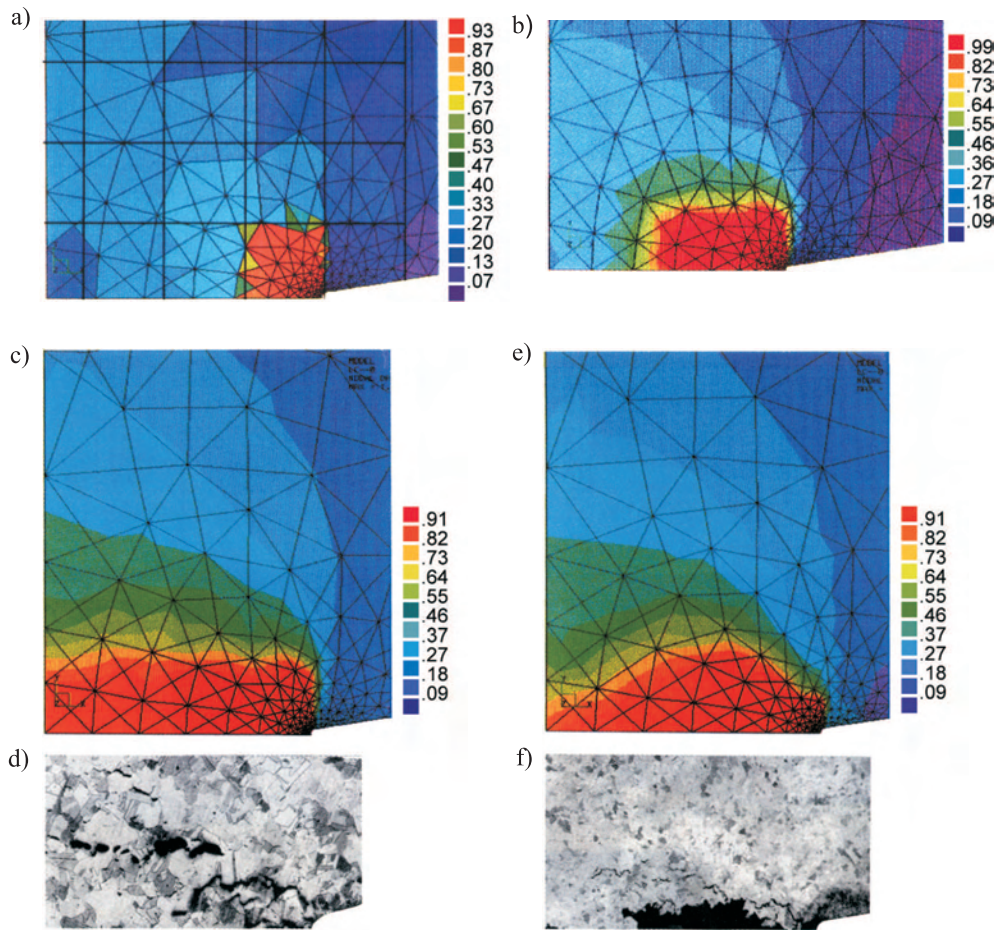


FIG. 6. Elemental colour damage plots for small and large, double externally cracked tension testpieces predicted using the finite domain non-local damage method; a) small testpiece just before failure of the first elements, the overlay grid shows location of cell mesh $t/t_r = 0.530$, b) small testpiece at $t/t_r = 0.822$, c) small testpiece at failure; d) mid-thickness micrograph of small testpiece close to failure; e) large testpiece at failure; and f) mid-thickness micrograph of large testpiece at failure.

It can be seen from Table 1 that the non-local continuum damage mechanics approach is capable of accurately predicting the observed experimental behaviour, provided that the finite element size and arrangement are confined to model damage over 6–7 material grains as a continuum property. In general, the requirement is that the length scales associated with the damage fields and spatial gradients be modelled to comply with the continuum theory.

4.1. CDM predictions of weldment failure

In the remainder of the paper, the use of CDM techniques are addressed for the prediction of creep damage initiation, growth, and failure in low alloy ferritic steel welds. This is done by consideration of the high-temperature creep constitutive equations for each material phase within the welded joint. Two-dimensional welds are first considered, followed by a more complex three-dimensional branched pressure vessel.

5. Background to CDM weldment studies

The remaining part of the paper concentrates on welded joints in low alloy ferritic materials which are typical of those used in steam pipework (i.e. the Cr Mo V steels and their usual weld metals). Welds have inhomogeneous materials properties which may be broadly categorised into five regions: the parent material, the so-called Type IV region, the Refined Heat Affected Zone (R-HAZ) the Coarse Grained HAZ (CG-HAZ) and the weld metal. In practice, the material behaviour in all five regions can be different and this will lead to extensive data requirements to characterise the material; this will include constitutive relations to describe creep deformation, creep rupture and the influence of multi-axial stress state.

Of particular concern in ferritic steel pipework is circumferential creep cracking in the extremity of the HAZ, adjacent to the untransformed parent pipe material, which experiences the lowest temperatures during welding, GOOCH AND KIMMINS [25]. This mode of failure, known as Type IV cracking, is particularly prevalent in steam pipework when the axial, or system stresses are significant, and it is the subject of the remainder of the paper.

5.1. Continuum damage mechanics modelling of creep failure in low alloy ferritic steel welds

HALL and HAYHURST [26] developed a CDM-based finite element (FE) solver, DAMAGE XX, which incorporates the physics of the creep deformation and rupture of the individual phases of the weld materials. This approach has been shown to predict successfully the deformation, damage, and failure history of the full-size pressure vessel weldment tests of COLEMAN *et al.* [27]. The research highlighted the important role of the difference in the creep characteristics of the weld metal, the heat-affected zone (HAZ) material, and the parent material. It was shown that the mismatch between material phases results in a marked redistribution of stress from the weld material into the HAZ and the parent material. Hence, the multi-axial stress rupture criterion due to HAYHURST [8] has an important role in further stress redistribution, in the determination of the damage distribution, and the predicted lifetime.

5.2. Experimental data used in this paper

An important series of tests on Cr Mo V pipework were conducted at the Marchwood Engineering Laboratories by COLEMAN and co-workers, c.f. [27] for example. These tests are used here to validate CDM prediction methods for welds. Data is taken from two data sources to compare CDM predictions with experimental results.

- (i) **For pipes:** An ERA Technology experimental database FAIRMAN [28] for pipes of the geometry given in Fig. 7 is used. Tests were undertaken at 848 °K, 873 °K, 893 °K and 913 °K with various ratios of axial to hoop stress. A low alloy steel combination of 0.5Cr 5Mo 0.25V pipe, welded with 2.25Cr 1Mo weld metal, was selected for the study. Pressures were selected to give test-times up to 12.871 h at 523 °K

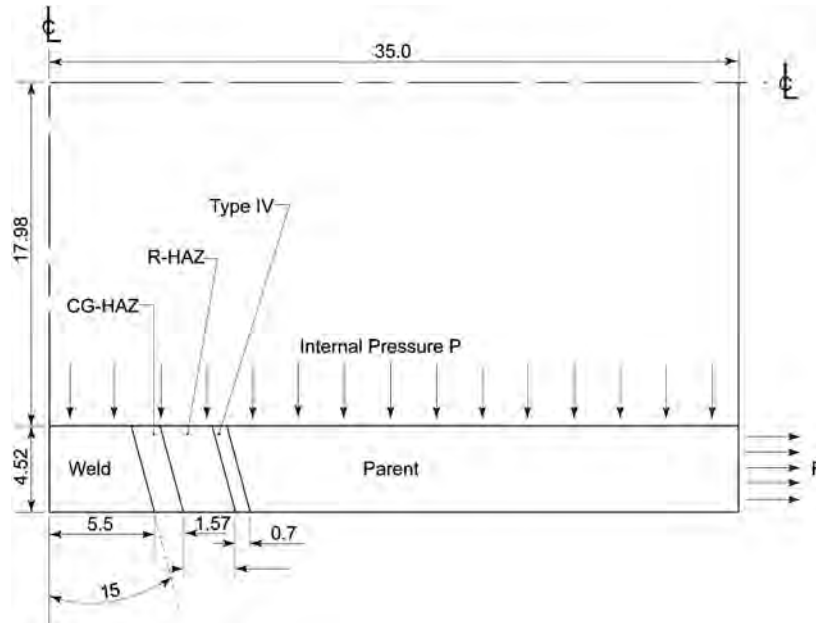


FIG. 7. Geometry of butt-welded pipe, applied internal pressure P (MPa) and independently applied end load F (N). Shown are the idealisations of Weld, Coarse Grained HAZ, Refined HAZ, Type IV, and Parent materials.

- (ii) **For cross-welded plates:** The ERA Technology experimental database FAIRMAN [28] is utilised for cross-weld testpieces, tested under an average minimum cross-section stress of 69.5 MPa at the three temperatures of 848 °K, 863 °K and 873 °K. The parent metal was 0.5Cr 5Mo 0.25V welded with matching 2.25Cr 1Mo weld metal. The geometry of the plates is given in Fig. 8.

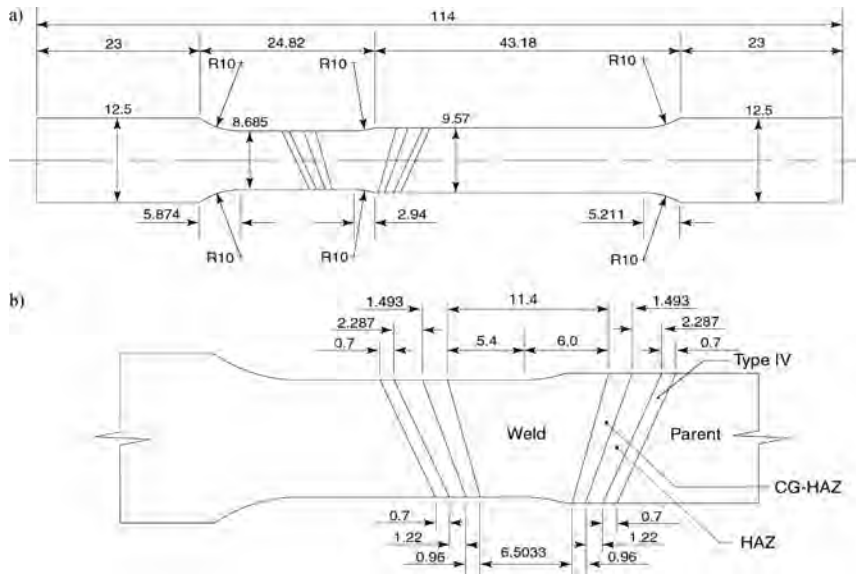


FIG. 8. Cross-weld test geometry showing a) overall testpiece dimensions in mm: and b) idealisation of Weld, Coarse Grained HAZ, Refined HAZ, Type IV, and Parent materials.

5.3. Calculations using CDM

CDM calculations using the Finite Element method have been undertaken using the 2-D Damage XX and the 3-D Damage XXX on the testpieces defined above. The important aspects of the analysis are the details of the finite element approach and, perhaps more importantly, the constitutive equations used. Both have been described extensively elsewhere and are summarised below for completeness.

5.3.1. Finite element calculations. In order to provide accurate predictions of the deformation and failure of components that operate in the creep regime, an analysis technique has been developed which combines the finite element method for structural analysis with constitutive equations that have been formulated within the framework of CDM by HAYHURST, DIMMER and CHERNUKA [14]; and HAYHURST, DIMMER and MORRISON [16]. Details of the finite element continuum damage mechanics method have been discussed by the latter [16], but basically a combined boundary-initial value problem has been solved using classical finite element techniques and a fourth-order Runge-Kutta numerical scheme to integrate the constitutive equations in the time domain. Application of the technique to butt welded pipes are described by VAKILI-TAHAMI *et al.* [29].

Table 2. Ferritic steel constitutive parameters at 863°K used by HAYHURST, VAKILI-TAHAMI and HAYHURST [36].

863°K	Parent	Weld	R-HAZ	Type IV	CG-HAZ
A (h^{-1})	1.3913×10^{-9}	2.8898×10^{-8}	1.3913×10^{-9}	5.2879×10^{-9}	1.5844×10^{-10}
B (MPa^{-1})	1.4337×10^{-1}	1.1109×10^{-1}	1.4337×10^{-1}	1.1762×10^{-1}	1.9746×10^{-1}
C (-)	2.9983	3.7894	2.9983	6.7693	8.8783
h (MPa)	7.3288×10^4	2.4649×10^4	7.3298×10^4	2.9714×10^4	6.2785×10^4
H^* (-)	0.4218	0.4088	0.4218	0.5430	0.6281
K_c (h^{-1})	1.0020×10^{-4}	5.2579×10^{-5}	1.0020×10^{-4}	6.3709×10^{-4}	1.4047×10^{-4}
ν (-)	2.8	2.7955	2.8	3.2192	2.7977

5.3.2. Constitutive Equations Constitutive equations developed by PERRIN and HAYHURST [30, 31] from the research of DYSON and co-workers [10, 32, 33, 34], have been utilised in the analysis. They are based on physical state variables which are used to describe the softening mechanisms that ferritic steels are known to suffer, namely: creep cavitation, ω , and the coarsening of the carbide precipitates, Φ . A state variable, H , is also used to describe the strain hardening that is associated with primary creep. The constitutive equations in multi-axial form that relate the creep strain rate, $\dot{\epsilon}_{ij}$, to the stress, σ_{ij} , and to the state variables are as follows:

$$(5.1) \quad \begin{aligned} \dot{\epsilon}_{ij} &= \frac{3s_{ij}}{2\sigma_e} A \sinh \left[\frac{B\sigma_e(1-H)}{(1-\Phi)(1-\omega)} \right], \\ \dot{H} &= (h\dot{\epsilon}_e/\sigma_e) (1 - (H/H^*)), \\ \dot{\Phi} &= (K_c/3) (1 - \Phi)^4, \\ \dot{\omega} &= CN\dot{\epsilon}_e (\sigma_1/\sigma_e)^\nu, \end{aligned}$$

where $N = 1$ for $\sigma_1 > 0$ and $N = 0$ for $\sigma_1 < 0$. The material parameters A, B, C, h, H^* and K_c define the uni-axial creep behaviour. Typical values of the material parameters, at the temperature of 863°K, are given in Table 2.

The expression controlling the multi-axial creep rupture criterion for Type IV materials only is as follows:

$$(5.2) \quad \nu = a \{ \exp (b\sigma_e/\sigma_o) \},$$

where values of the empirical factors a and b are given in Table 3 for the three relevant temperatures; and, σ_o is the uni-axial stress (MPa) required to give a lifetime of 1000 h.

Table 3. Parameters a and b used to determine the multi-axial stress rupture parameter ν in the equation $\nu = a \{\exp (b\sigma_e/\sigma_o)\}$ for the Type IV material.

Parameter	Temperature		
	848°K	863°K	873°K
a	2.3373	2.2133	2.1137
b	2.1287	1.9861	1.8689

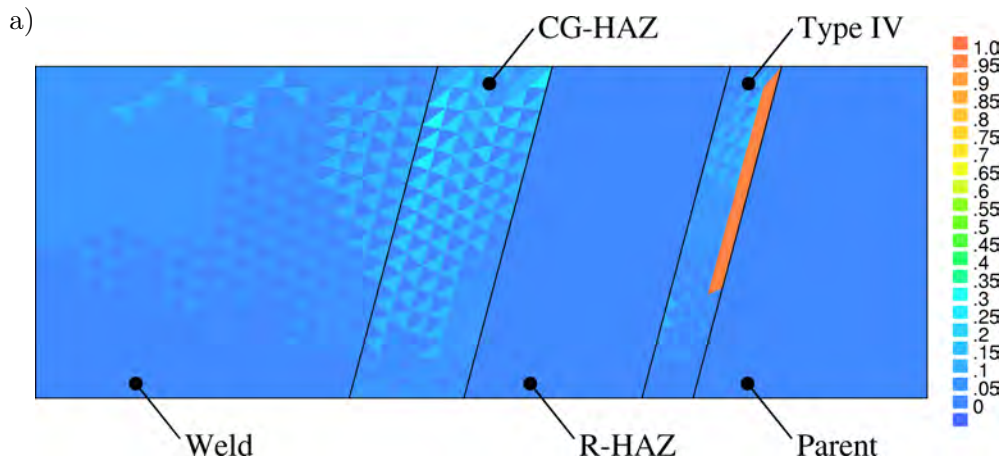
6. CDM predictions: butt-welded pipes and cross-welded tension plates

CDM analyses of butt-welded pipes and cross-welded tension plates have been carried out using the methods described in Sec. 6 with the constitutive Eq. (5.1). Constitutive parameters for 863°K are given in Table 2, and for 848°K, 873°K, and 893°K in HAYHURST *et al.* [35]. Examination of Table 2 shows that the constitutive parameters for the R-HAZ and the parent materials have been assumed to be the same. This assumption has been made because no test data is available for the R-HAZ region; and, since its fine-grained, bainite microstructure [35] closely resembles that of the parent material. Determination of the constitutive parameters has been carried out using methods developed by KOWALEWSKI *et al.* [36]; these involve the definition of an error optimization functional using the difference between predicted and experimental creep strains. In the numerical optimization, the values of the constitutive parameters are sought which minimize the error functional. In order to avoid local minima, the constitutive parameters were sequentially determined; first for primary, then with secondary, and finally including tertiary creep strains. These techniques have been used by MUSTATA and HAYHURST [37] and by HAYHURST *et al.* [38, 39]; they have also used property ratio techniques for those temperatures and materials where experimental data is limited. Values of the multi-axial parameter, ν , for the Type IV region, are given by Eq. (5.2) and the data of Table 3. The results of the CDM analyses on butt-welded pipes and cross-welded tension plates are now presented.

6.1. CDM analyses of pipes

Predicted damage fields, made using axi-symmetric finite elements, on a diametral section of a butt-welded pipe at a life fraction of 99%, Fig. 9(a), are compared with a surface macrograph in Fig. 9(b). The left-hand sides of both figures denote the mid-plane of the weld. Failure is clearly predicted to occur in the Type IV region with a modest level of damage in the Coarse Grained HAZ region $\omega \approx 0.33$.

Detailed comparison of lifetime predictions with the experimental data are given in Fig. 10 for test temperatures of 848 °K, 863 °K and 873 °K; it may be seen that the analysis gives a very precise description of the experimental data.



b)

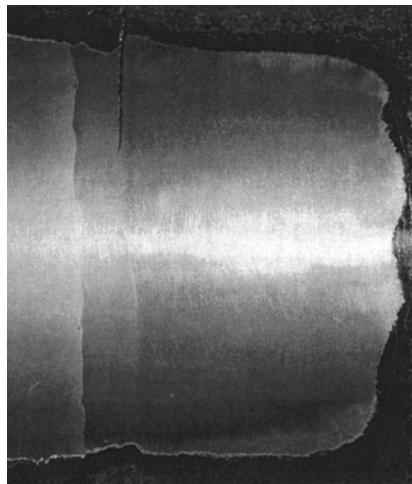


FIG. 9. Comparison of predicted damage fields close to failure $t/t_r = 0.99$, for (a) a diametral cross-section of a butt-welded pipe subjected to an internal pressure of 15.544 MPa and an end load of 24.232 kN at 873 °K, the left-hand edge of the figure is the weld centre line, with (b) a macrograph taken from the surface of the failed testpiece.

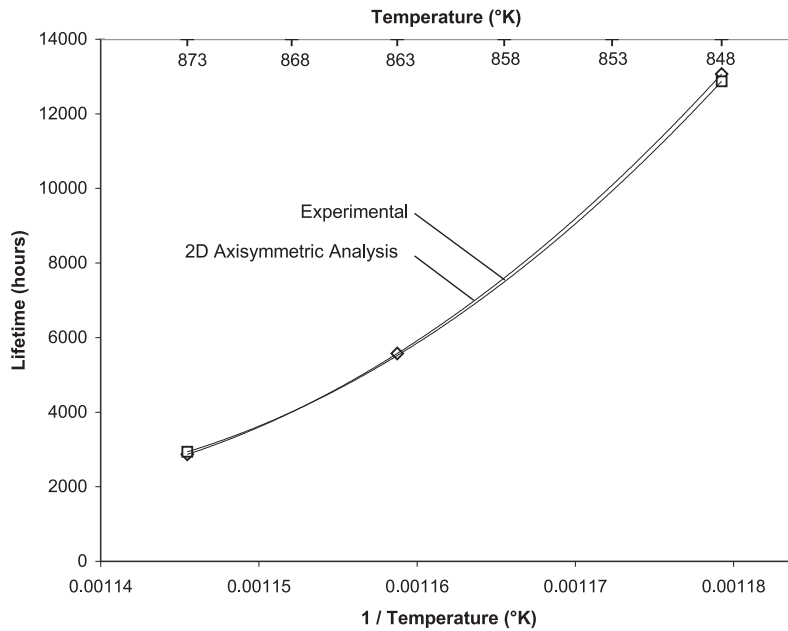


FIG. 10. Comparison of butt-welded pipe lifetimes predicted using two-dimensional axi-symmetric CDM analyses at 848 °K, 863 °K, 873 °K with experimental results. Squares denote experiments, and diamonds the analytical values.

6.2. CDM analyses of cross-welded tension plates

Predicted damage fields, made using both the plane strain two-dimensional finite elements, and three-dimensional finite elements, with plane strain boundary conditions imposed, are shown in Fig. 11(a) and Fig. 11(b) respectively, at a life fraction of 99%. In both cases failure is predicted to occur in the Type IV region contained within the smaller cross-section. There is little evidence of damage in the Coarse-Grained HAZ region. These predictions compare well with the macrograph of Fig. 11(c).

Predictions of lifetime for both 2-D and 3-D plane strain conditions are made in Fig. 12 with the results of experiments for 848°K, and 873°K. It may be seen that, although the finite element size is nearly identical, the predicted results bound the experimental results with little error.

6.3. Comment

The CDM predictions of lifetimes and damage fields are accurate and reliable for the butt-welded pipes and cross-welded tension plates, provided that the boundary conditions are known and the materials data requirements can be met.

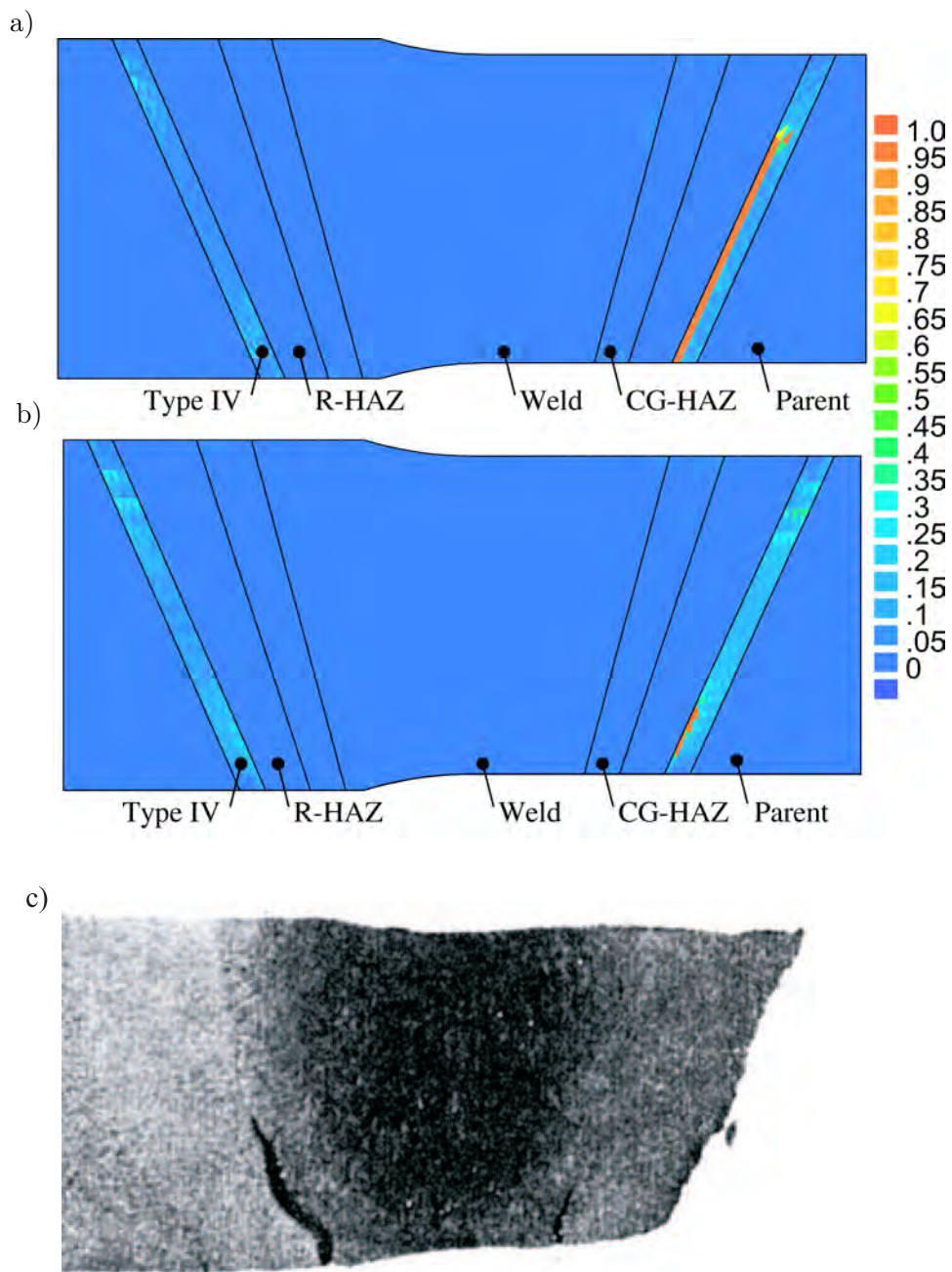


FIG. 11. Comparison of predicted damage fields close to failure $t/t_r = 0.99$, for (a) two-dimensional and for (b) three-dimensional plane strain uni-axially loaded cross-weld testpieces at 873 °K at an average minimum cross-section stress of 69.5 MPa, with (c) a micrograph taken from a failed testpiece. Testpiece failure takes place in the Type IV region.

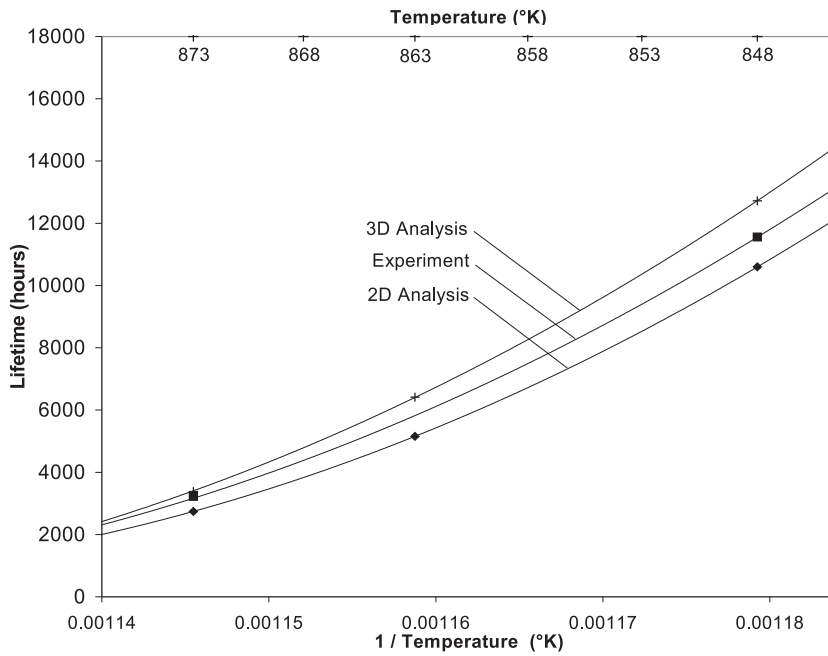


FIG. 12. Comparison of predicted lifetimes for two- and three-dimensional plane strain CDM analyses at 848 °K, 863 °K and 873 °K with experimental results at 848 °K and 873 °K for an average minimum cross-section stress of 69.5 MPa.

7. CDM predictions of creep failure in a branched welded pressure vessel

The paper now addresses the use of CDM techniques to predict the behaviour of a complex 3-D weldment.

7.1. Test conditions, material and main vessel geometry

The medium bore 0.5Cr, 0.5Mo, 0.25V parent main pipe was welded using 2.25Cr, 1Mo material to the parent material branch to form the cylinder-cylinder intersection, c.f. Fig. 13(a). The main body of the vessel (pipe) was 465 mm in outer diameter with a wall thickness of 20 mm; the branch was 111 mm in inner-diameter with a wall thickness of 8 mm. The mean radius to thickness ratio of the main pipe $R/t_p = 11.125$, and the mean radius to thickness ratio of the branch $r/t_b = 7.438$. Both the main pipe and branch were pressurised to a constant level of 4.0 MPa, at a constant uniform temperature of 863 °K. The internal pressure generates a main pipe mean diameter hoop stress PR/t , of 44.5 MPa. The parent and weld materials have the same Young's modulus of 160 GPa at 863 °K.

The weld geometry was specified at two geometrical locations, namely the crotch and flank sections. The crotch plane contains the axes of both the main pipe and branch; Fig. 13(a) defines two such, diametrically opposite locations as 0° and 180° . The flank plane is normal to the crotch plane, and contains the axis of the branch; and, Fig. 13(b) shows the finite element brick idealization of one quarter of the branched vessel.

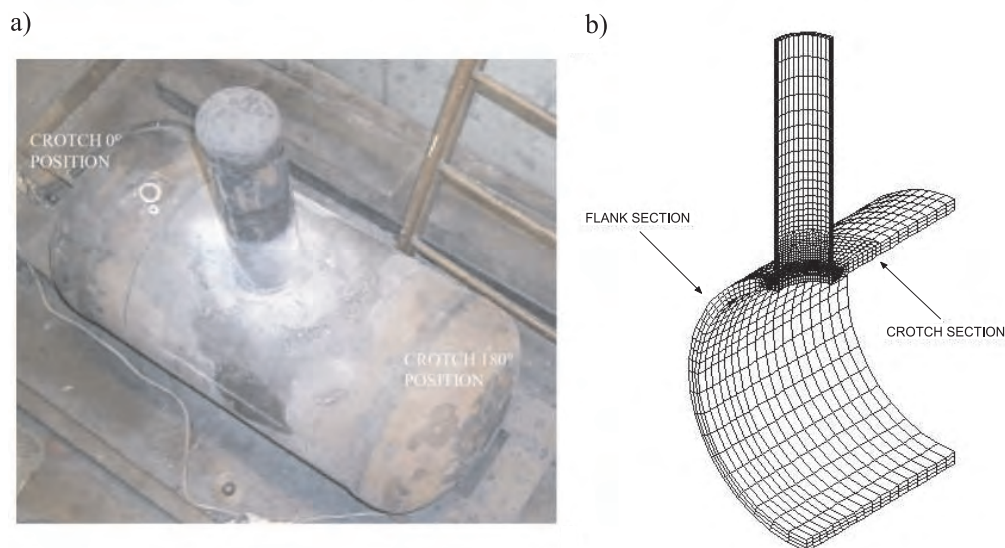


FIG. 13. Medium bore branch tested at a constant pressure of 4 MPa at 863 °K (a), and finite element brick mesh of a single quadrant of the vessel (b).

The geometry of the weld on the flank section is shown in Fig. 14(a). The details of how the weld, CG-HAZ, R-HAZ and Type IV materials interface with the main pipe are shown in Fig. 14(b). The geometry of the weld on the crotch section is shown in Fig. 14(c). Following HAYHURST, VAKILI-TAHAMI, MUSTATA and HAYHURST [39], the Type IV thickness was taken to be 0.7 mm.

7.2. Weld geometry

The testing procedures for the vessel shown in Fig. 13(a) have been reported by PATEL [40, 41] and the results of post-testing metallographic investigation have been presented by CHILCOTT [42]. Independent metallographic examinations of both the crotch and flank weldments sections have been carried out; and, the resultant macrographs have been used to determine the mean CG-HAZ thickness at different locations.

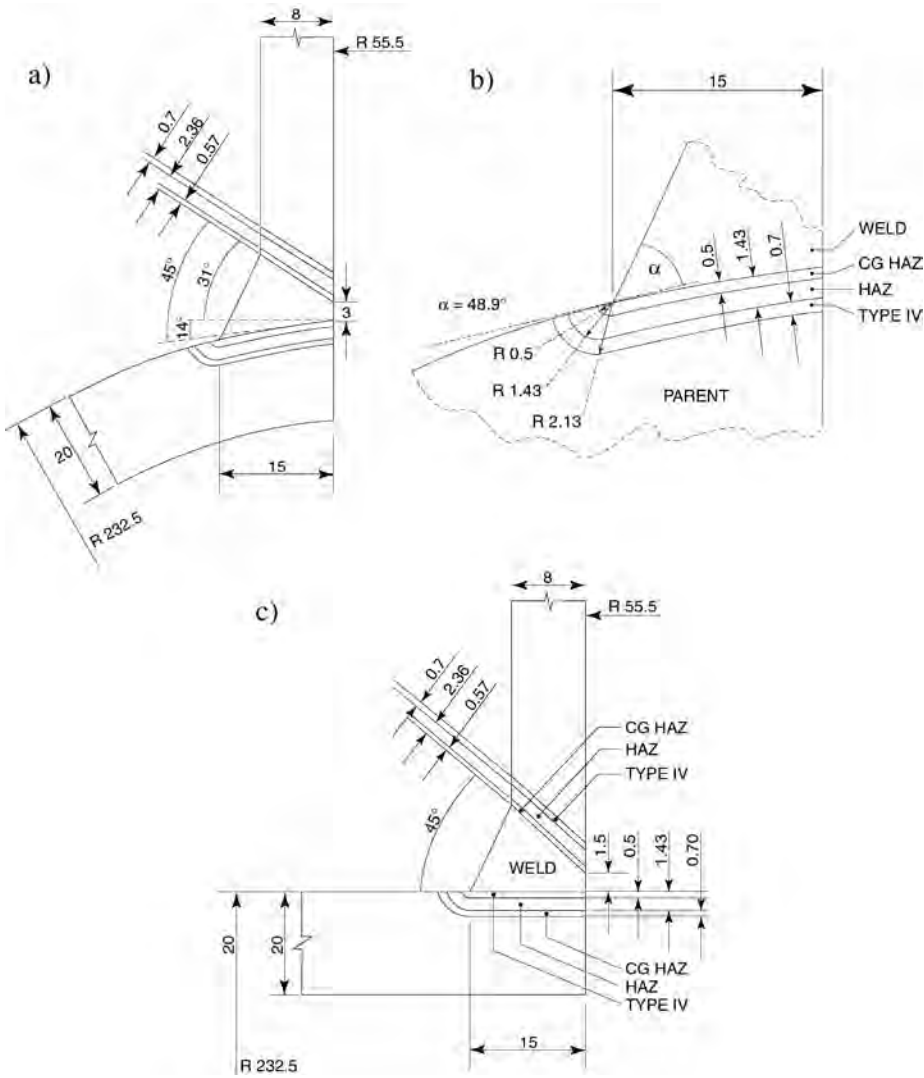


FIG. 14. Weld geometry detail shown on the flank section (a), (b) and on the crotch section (c).

7.3. Constitutive equations

The constitutive Eq. set (5.1) has been used with parameters calibrated for 863 °K. The set of constitutive parameters reported by HAYHURST, MUSTATA and HAYHURST [38] will be used for 863 °K cf. Table 2. HAYHURST, VAKILI-TAHAMI, MUSTATA and HAYHURST [43] have shown that the multi-axial stress rupture parameter for the Type IV material is $\nu = 3.2192$; it is given by Eq. (5.2),

the data in Table 2, $\sigma_e = 25.76$ MPa being the branch membrane stress calculated for the mean branch diameter; and $\sigma_o = 136.58$ MPa.

7.4. Finite element idealisation of branch

A single quadrant of symmetry of the branch is shown in Fig. 13(b); the planes of symmetry are the flank and crotch planes. The volume has been modelled with six-sided bricks, each brick is then filled with 24 constant strain tetrahedra; the total number of nodes is 54 687, the number of degrees of freedom is 164 061 and the number of elements is 240 048. Details of the finite element calculations are given by HAYHURST, HAYHURST and VAKILI-TAHAMI [43].

8. Presentation of the branch CDM results

The results of the CDM calculations are now presented for the branch using the constitutive Eq. (5.1) for the five material models with CG-HAZ. Failure was predicted to take place in the main pipe Type IV region, and damage fields are given in Fig. 15. Initially the damage grows from crotch $\theta = 0^\circ$ towards the flank plane and is shown in Fig. 15(a) at the life fraction $t/t_r = 0.81$. At the life fraction $t/t_r = 0.94$, shown in Fig. 15(b), damage has grown halfway through the main pipe Type IV region. In Fig. 15(c) damage can be seen to have grown through the pipe wall. Shown in Fig. 16 are damage contour plots of diametral sections of the branch close to failure at the life fraction $t/t_r = 0.99$; both the branch and main pipe Type IV regions are shown. Figure 16(a) is the crotch section; Fig. 16(b) is a section on the plane defined by $\theta = 22^\circ$ and, Fig. 16(c) is the flank section. Figure 16(a) shows failure to take place in the main pipe Type IV region, with damage localised at the weld toe in the CG-HAZ region. The weld toe CG-HAZ damage formed very early in life and spread from crotch to flank very quickly, the reason for this is that it provides a stress relief mechanism; but, having relieved the stress, the CG-HAZ damage is benign and does not propagate until near end of life. Growth of damage then predominates in the Type IV region; however, evidence of linkage between CG-HAZ and Type IV damage through the main pipe R-HAZ is apparent.

Intense damage may be observed in Figs. 16(a) and 16(b) in the branch CG-HAZ, and some evidence of “fusion boundary” damage in the adjacent weld region, although this occurs near the end of life. Figure 16(b) shows damage on the diametral plane defined by $\theta = 22^\circ$ and its location is shown in Fig. 15(c); this plane has been selected since it resides between the regions of dominant Type IV damage in the branch and main pipe as indicated in Fig. 15. Sub-surface damage can be seen in the branch Type IV region, Fig. 16(b); CG-HAZ damage at both weld toes is evident; a predominance of main pipe Type IV

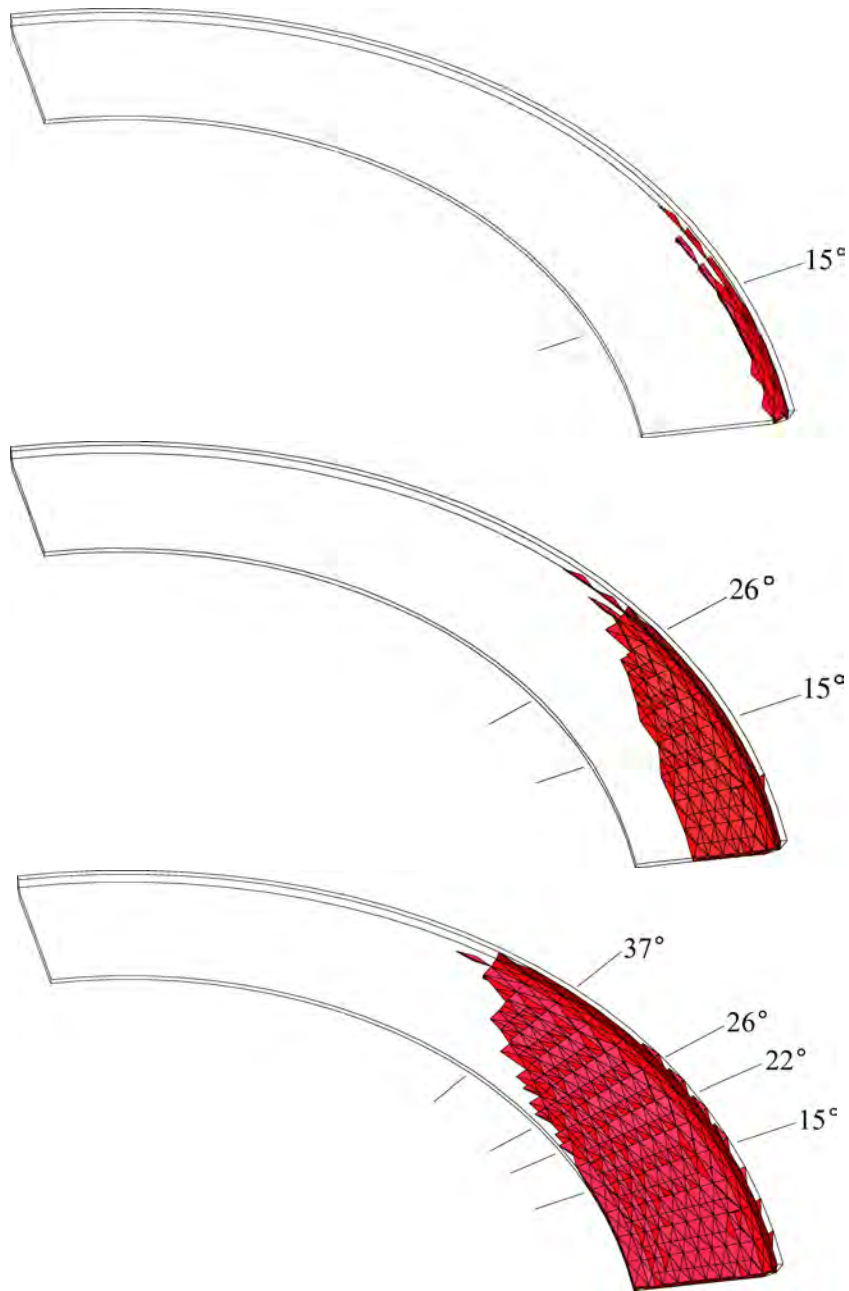


FIG. 15. Distribution of failed elements in the Type IV region of the pipe predicted using constitutive parameters employed by HAYHURST, VAKILI-TAHAMI, and HAYHURST [35] for the four material models at: (a) $t/t_r = 0.81$; (b) $t/t_r = 0.94$; $t/t_r = 0.99$. The right-hand side of the figure shows the crotch plane $\theta = 0^\circ$ and the left-hand side the flank plane $\theta = 90^\circ$.

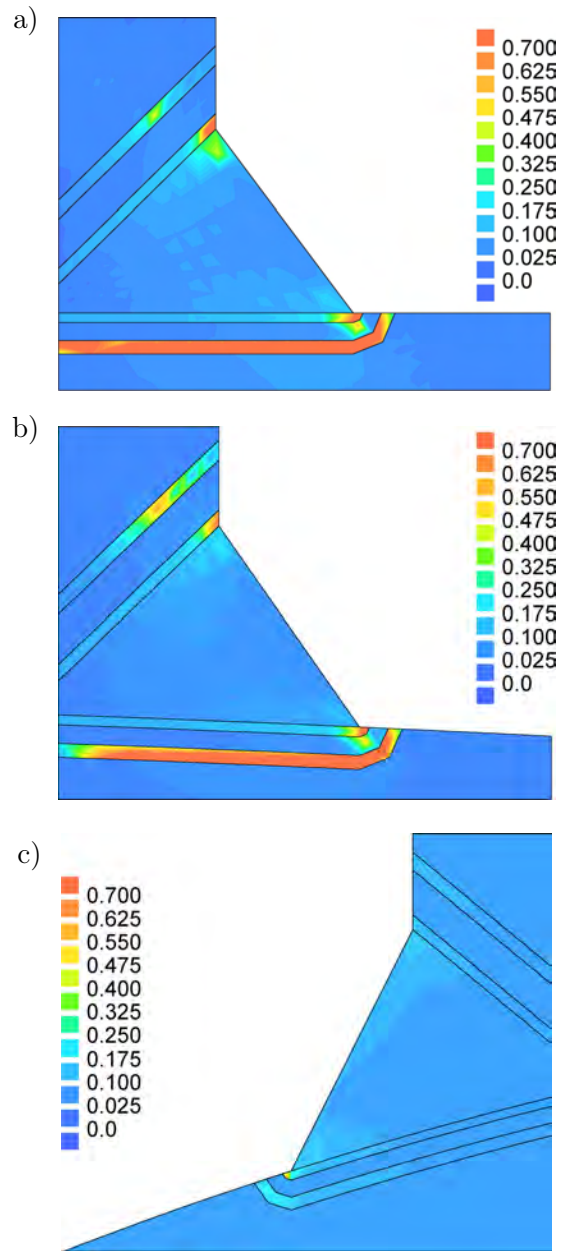


FIG. 16. Damage contour plots predicted for diametral sections of the branch at $t/t_r = 0.99$ for the five material model. Angular locations of the sections shown are defined relative to the crotch plane $\theta = 0^\circ$. Figure (a) denotes the crotch section, figure (b) denotes a section on a diametral plane located at $\theta = 22^\circ$ to the crotch plane; and figure (c) denotes the flank section $\theta = 90^\circ$.

damage can be seen; and, evidence of linkage between CG-HAZ and Type IV damage through the main pipe R-HAZ is apparent. Figure 16(c) for the flank section shows no evidence of damage other than the initial CG-HAZ damage referred to earlier.

9. Comparison of damage predictions with the results of micro-structural examinations of tested vessel

Detailed tested vessel examination reports have been presented by PATEL [40] and by CHILCOTT [42]. The first observation is that lifetime predicted by the five material models, 18 242 h, is conservative and in good agreement with the experimental lifetime of 20 038 h, with an error of 9%.

With regard to the location of the first damage, and its development through the thickness of the vessel, these have been reported by PATEL [40, 41] and CHILCOTT [42]. Detailed metallurgical examination confirmed that leakage took place due to the two crotch defects located close to the weld toes in the main pipe. The cracks propagated at the two locations in the crotch plane, within the CG-HAZ on the main pipe side of the weld. Significant defects were also observed in the Type IV zones on the main pipe side of the weld; and, also on the branch side of the weld.

With regard to the predictions, Fig. 16(a) shows damage growth from the weld toe R-HAZ and CG-HAZ regions in the main pipe; however, spread of damage to the parent material is not predicted. Failure on the inner bore is predicted to be within the Type IV region, Figs. 15(c) and 16(a), with no evidence of damage in the parent, R-HAZ and weld materials.

In summary, the metallographic evidence provides confirmation that the five materials analyses correctly predict crotch plane failure in the main pipe Type IV. Also, that the steam leakage path is correctly determined to be from the inner bore crotch plane locations, along the Type IV regions, through the R-HAZ regions close to the weld toe, to produce leakage through the CG-HAZ and Type IV regions at the weld toe.

10. Conclusions

1. It is shown how CDM techniques can be used to predict the creep rupture behaviour of a wide range of structures, varying in complexity from simple bars to creep crack growth situations.
2. Size effects associated with cracks growing in plane strain members can be predicted by the inclusion of a length scale in the Continuum Damage Mechanics analysis. The proviso being that the length scales associated with the damage fields and gradients be modelled to comply with continuum theory.

3. It has been shown how the creep rupture behaviour of the 2-D welds, butt-welded pipes and cross-welded tension specimens, which are composed of five different materials, can be accurately predicted using CDM techniques. Knowledge is required of the constitutive equations and parameters, in particular the multi-axial stress rupture criteria.
4. Creep rupture, damage initiation, its evolution and spread in the form of a creep crack in the 3-D weldment of a branched pressure vessel have been accurately predicted using the CDM techniques. The same material constitutive equation requirements as for 2-D welds, the requirement that length scales associated with damage fields and gradients be correctly modelled using finite element methods, and the need for considerable computational requirements, had all to be met. Despite the latter requirements, accurate lifetimes and the correct failure modes have been predicted.

Acknowledgments

The CDM weldment computations were carried out by R. J. Hayhurst, who acknowledges funding provided by EPSRC, (RAIS) during secondment from UMIST (now The University of Manchester) to British Energy, Barnwood. The provision of creep data and metallographic information, together with support regarding data interpretation, by Dr D. Dean and Mr M. Spindler of British Energy Barnwood, Gloucester, is gratefully acknowledged. Acknowledgement for permission to publish the creep test results is given to the sponsors of the ERA Technology Project – 4080 from which the data originates, in particular ALSTOM Power (UK) Ltd, British Energy plc, and PowerGen plc. The provision of EPSRC, CSAR, computer resource on the Silicon Graphics Origin 2000 (Fermat) is gratefully acknowledged. The final stages of this paper were finalised whilst the author was on sabbatical leave at The Materials and Mechanical Engineering Departments, University of California at Santa Barbara, USA; he acknowledges financial support provided, through a Global Research Award, by The Royal Academy of Engineering of the United Kingdom.

References

1. BRITISH STANDARDS INSTITUTION, *Specification for design and construction of ferrous piping installations for and in connection with land boilers*, BS 806, 1993.
2. BRITISH STANDARDS INSTITUTION, *Specification for design and manufacture of water-tube steam generating plant (including superheaters, reheaters and steel tube economisers)*, BS 1113, 1989.
3. BRITISH STANDARDS INSTITUTION BSi PD 5500, *Specification for unfired fusion welded pressure vessels*, BSi PD 5500: 2003

4. ASME, BOILER PRESSURE VESSEL CODE, CODE CASE: NUCLEAR COMPONENTS, CASE N-47-29 class 1 components in elevated temperature service, Section II, Division 1, 1990.
5. R5 ISSUE 3, *Assessment procedures for the high temperature response of structures*, British Energy Generation Ltd, Gloucester, UK., 2003.
6. J. R. RICE, *Mathematical analysis in the mechanics of fracture – an advantised treatise*, H. LIEBOWITZ [Ed.], II, Academic Press, 1968.
7. D. R. HAYHURST, C. J. MORRISON and P. R. BROWN, *Creep crack growth*, Proceedings of the 3rd IUTAM Symposium, Creep in Structures, Leicester UK, 1980, 564–574, Springer-Verlag, Berlin, Heidelberg, New York 1981.
8. D. R. HAYHURST, *Creep rupture under multi-axial states of stress*, J. Mech. Phys. Solids, **20**, 381–390, 1972.
9. D. R. HAYHURST, *Engineering approaches to high-temperature design*, Chap. 3, Pineridge Press, Swansea 1983.
10. M. OTHMAN, D. R. HAYHURST and B. F. DYSON, *Skeletal point stresses in circumferentially notched tensions bars undergoing tertiary creep modelled with physically-based constitutive equations*, Proc. R. Soc. Lond. A. **441**, 343–358, 1993.
11. D. R. HAYHURST, *Materials data bases and mechanisms-based constitutive equations for use in design*, 167–205, Chapter [in:] *Creep Damage in Materials and Structures*, A. ALTENBACH and J. J. SKRZYPEK, Springer-Wein, New York 1999.
12. D. R. HAYHURST, *Materials data requirements for computer simulation in design and manufacturing*, Chap. 4. *Computer-aided-design and new materials*, 189–224, [in:] J-P. CALISTE, A. TRUYOL and J. WESTBROOK [Eds.], *Thermodynamic modelling and materials data engineering*, Springer, Berlin, Heidelberg 1998.
13. D. R. HAYHURST, *Stress redistribution and rupture due to creep in a uniformly stretched thin plate containing a circular hole*, J. Appl. Mech., **40**, 244–256, 1973.
14. D. R. HAYHURST, P. R. DIMMER and M. W. CHERNUKA, *Estimates of the creep rupture lifetime of structures using the finite element method*, J. Mech. Phys. Solids, **23**, 335–355, 1975.
15. D. R. HAYHURST and B. STORAKERS, *Creep rupture of the andrade shear disc*, Proc. R. Soc. Lond. A., **349**, 369–382, 1976.
16. D. R. HAYHURST, P. R. DIMMER and C. J. MORRISON, *Development of continuum damage in the creep rupture of notch bars*, Phil. Trans. Roy. Soc. Lond. A., **316**, 103–129, 1984.
17. D. R. HAYHURST, *Creep continuum damage mechanics: A unifying theme in high-temperature design*, High-Temperature Structural Design, ESIS 12, L. H. LARSON [Ed.], Mechanical Engineering Publications, London, 317–334, 1992.
18. D. R. HAYHURST, C. J. MORRISON and F. A. LECKIE, *The effects of stress concentrations on the creep-rupture of tension panels*, J. Appl. Mech., **42**, 61–618, 1975.
19. W. GOODALL and R. A. AINSWORTH, *Failure of structure by creep*, Proc. 3rd Int. Conf. Press. Vess. Tech., Tokyo, vol. II, ASME, 871–882, 1977.
20. V. P. SDOBYREV, *Long-term strength of alloy EI-437B under complex stresses*, Izv. Akad. Nauk SSSR, Otd. Tech. Nauk **4**, 92, 1958.

21. P. W. BRIDGMAN, *Large plastic flow and fracture*, McGraw Hill, New York 1952.
22. D. R. HAYHURST, P. R. BROWN and C. J. MORRISON, *The role of continuum damage in creep crack growth*, Phil. Trans. R. Soc. A., Lond, **311**, 131–158, 1984.
23. F. R. HALL, D. R. HAYHURST and P. R. BROWN, *Prediction of plane-strain creep-crack growth using continuum damage mechanics*, Int. Jnl. Damage Mech., **15**, 353–383, 1996.
24. F. R. HALL and D. R. HAYHURST, *Modelling of grain size effects in creep crack growth using a non-local continuum damage approach*, Proc. R. Soc. Lond. A, **433**, 405–421, 1991.
25. D. J. GOOCH and S. T. KIMMINS, *Type IV Cracking in 0. Cr 0.5Mo 0.25V/2.25Cr 1Mo weldments*, [in:] B. Wilshire, R. W. Evans, Proceedings of the Third International Conference on Creep and Fatigue of Engineering Materials and Structures, Swansea 1987.
26. F. R. HALL and D. R. HAYHURST, *Continuum damage mechanics modeling of high-temperature deformation and failure in a pipe weldment*. Proc. R. Soc. Lond., A **433**, 383, 1991.
27. M. C. COLEMAN, J. D. PARKER and D. J. WALTERS, *The behaviour of ferritic weldments in thick section 0.5Cr 0.5Mo 0.25V pipe at elevated temperature*. Int. J. Pressure Vessels and Piping, **18**, 277, 1985.
28. A. FAIRMAN, ERA Project 4080, *The industry creep programme, materials/analysis panel*, Preliminary metallographic findings of failed 0.5Mo V uni-axial cross-welded testpieces, ERA Report No. MAP/64/95, 1995.
29. F. VAKILI-TAHAMI, D. R. HAYHURST and M. T. WONG, *High-temperature creep rupture of low alloy ferritic steel butt-welded pipes subjected to combined internal pressure and end loadings*, Chapter 5 [in:] Reference Stress Methods – Analysing Safety and Design, IAN W. GOODALL [Ed.], IMechE., Professional Eng. Pub., Bury St Edmunds and London 2003.
30. I. J. PERRIN, and D. R. HAYHURST, *Creep constitutive equations for a 0.5 Cr 0.5 Mo 0.25 V ferritic steel in the temperature range 600° C to 675° C*, J. Strain Anal., **31**, 299–314, 1996.
31. I. J. PERRIN and D. R. HAYHURST, *Continuum damage mechanics analyses of Type IV creep failure in ferritic steel cross-weld specimens*. Int. J. Press Vessels and Piping, **76**, 599, 1999.
32. B. F. DYSON, A. K. VERMA and Z. C. SZKOPIAK, *The influence of stress state on creep resistance; experiments and modelling*, Acta Metall., **29**, 1573–1580, 1981.
33. B. F. DYSON and D. MCLEAN, *Particle-coarsening, σ_0 , and tertiary creep*, Acta Met., **30**, 17–27, 1983.
34. B. F. DYSON, *Creep fracture of metals: mechanisms and mechanics*, Rev. Phys. Appl., **23**, 605–613, 1988.
35. R. J. HAYHURST, F. VAKILI-TAHAMI and D. R. HAYHURST, *Type IV and coarse grained haz creep rupture of ferritic steel uni-axially loaded crossweld testpieces: verification of 3-D parallel CDM software, DAMAGE XXX using 2-D analyses and experiments*, UMIST RESEARCH REPORT No: DMM. 03. 01 (revised), 2004.
36. Z. L. KOWALEWSKI, D. R. HAYHURST and B. F. DYSON, *Mechanisms-based creep constitutive equations for an aluminium alloy*, J. Strain Anal., **29**, 309–316, 1994.

37. R. MUSTATA and D.R. HAYHURST, *Creep constitutive equations for a 0.5Cr 0.5Mo 0.25V ferritic steel in the temperature range 565°C – 675°C*, Int. Jnl. Press. Vess. and Piping, **82**, 363–372, 2005.
38. R. J. HAYHURST, R. MUSTATA and D. R. HAYHURST, *Creep constitutive equations for Parent, Type IV, R-HAZ and weld material in the range 565–640°C for Cr-Mo-V weldments*, Int. Jnl. Press. Vess. and Piping, **82**, 137–144, 2005.
39. R. J. HAYHURST, F. VAKILI-TAHAMI, R. MUSTATA and D. R. HAYHURST, *Thickness and multi-axial stress rupture criteria of the type iv component of a ferritic steel weld*, Jnl. Strain Analysis, **39**, 6, 729–743, 2004.
40. G. PATEL, *R5 medium bore branch life assessment*, British Energy, Barnwood, Report E/REP/A TEC/005/GEN/01, 2002.
41. G. PATEL, *Creep life assessment of weld trunion and branch components using the R5 procedure*, Int. J. Pressure Vess and Piping, **80**, 695–704, 2003.
42. S. M. CHILCOTT, *Private communication, Re: Metallurgical examination of a medium bore branch vessel after testing at elevated temperature and pressure*, Confidential British Energy Engineering Division Report: E/EAN/MATS/0024/AGR/01, July 2001.
43. D. R. HAYHURST, R. J. HAYHURST and F. VAKILI-TAHAMI, *CDM predictions of creep damage initiation and growth in ferritic steel weldments in a medium bore branched pipe under constant pressure at 590C using a 5-material model*, to appear: Proc. R. Soc. Lond.

Received September 16, 2004; revised version January 14, 2005.
